

BALANCING THE RELIABILITY AND COST OF ENERGY SYSTEMS UNDER GRID AND COMPONENT FAILURES THROUGH PARETO-OPTIMAL STORAGE OPERATION

Benedict Brosius¹, Dustin Frings¹, Benedikt Nilges¹, Niklas von der Assen^{1*}

¹ Institute of Technical Thermodynamics, RWTH Aachen University, Aachen, Germany

*Corresponding Author: niklas.vonderassen@itt.rwth-aachen.de

ABSTRACT

In distributed multi-energy systems, the reliability of energy supply is threatened by unplanned failures of grid utilities and energy system components. To improve reliability, thermal energy storages can be integrated. In addition to improving reliability, thermal energy storages reduce operating costs, e.g., by capitalizing on electricity price fluctuations. However, existing storage operation methods neglect the inherent trade-off between reliability and costs. In contrast, our study presents a method to balance both objectives. Our method extends a cost-optimization problem with an approximation of the Expected Energy Not Served, a widely used reliability metric. To solve the resulting bi-objective problem, we employ a self-adjusting weighted sum algorithm that generates Pareto-optimal operating schedules. Finally, we validate the reliability of these operating schedules in a Monte Carlo reliability assessment. In an industrial case study, we benchmark our method against a state-of-the-art operation method. In comparison, our method reduces undersupply by 19.2 % and operating costs by 1.5 %. Consequently, our method can improve both the reliability and costs of distributed multi-energy systems with storages.

1 INTRODUCTION

Thermal energy storages are frequently integrated into distributed multi-energy systems (DMES) to improve both the reliability of energy supply and operating costs. Reliability is threatened by failures of grid utilities such as electricity, and energy system components such as heat pumps. Storages not only mitigate the undersupply caused by these failures, but also reduce operating costs, e.g., by exploiting time-varying electricity prices. However, reliability and costs are partially conflicting objectives: Maximizing reliability requires retention of storage reserves while minimizing costs results in frequent charging and discharging cycles. As both objectives are crucial for stakeholders, DMES operators must carefully balance this trade-off.

Currently, there are limited optimization methods available to consider both reliability and cost when operating storages in DMES. Methods typically neglect component failures (Pazouki et al. 2014) or assume that storages can operate with perfect foresight of the exact timing of these failures (Guo und Zhao 2018). However, perfect foresight of failures is infeasible in practice. Ren et al. (2022) propose an operating method which avoids perfect foresight while considering failures of the electricity and gas grids. For each time step within the operation horizon, their method determines the minimum storage levels required to meet critical demands if a failure occurs at that time step. Subsequently, they constrain these minimum storage levels in a cost-optimization problem to generate highly reliable operating schedules. However, they disregard that reducing reliability could improve cost.

In this work, we propose a method to balance the reliability and cost of DMES with thermal storages under grid and component failures. The method quantifies reliability with the Expected Energy Not Served (EENS), a widely used metric for energy system reliability. First, we approximate the EENS as a function of the storage levels at each time step. Then, we incorporate this EENS approximation into a bi-objective optimization model to generate Pareto-optimal operating schedules. Finally, we

reevaluate the EENS of these schedules in a Monte Carlo reliability assessment (MCA). The MCA simulates random grid and component failures and optimizes the reaction of the energy system to these failures. Unlike existing MCAs (Ren et al. 2022), the proposed MCA avoids perfect foresight of future failures.

The paper is structured as follows. Section 2 introduces an energy system optimization model for the cost-optimal operation of DMES, on which we base our method. Furthermore, Section 2 presents a state-of-the-art method to increase the reliability of energy supply. Section 3 proposes our method to balance reliability and cost. Section 4 presents an industrial case study, where we compare the proposed method to the state-of-the-art method. Finally, we draw conclusions in Section 5.

2 OPERATIONAL OPTIMIZATION OF ENERGY SYSTEMS

2.1 Operational cost-optimization model

In this section, we describe the cost-optimization model, on which our proposed method is based. We refer to this cost-optimization model as the base model. Similar optimization models are frequently used to operate energy systems. For readability, we write optimization parameters in regular font and optimization variables in bold font. The objective of the base model is as follows: Given exogenous heating, cooling, and electricity demands, capacities of energy system components, grid import costs and component operating costs, minimize the energy system operating costs (OPEX):

$$\min \text{OPEX} = \min \sum_{t \in \mathcal{T}} \Delta_t \cdot \left(\sum_{b \in \mathcal{B}} \mathbf{G}_{b,t} k_{b,t}^{\text{import}} + \sum_{p \in \mathcal{P}} \mathbf{P}_{p,b_{\text{ref}}(p),t} k_p^{\text{operation}} \right) \quad (1)$$

The OPEX consists of grid import costs, and operating costs of production components. At every time step t within the yearly operating horizon \mathcal{T} , the grid import cost of a product $b \in \mathcal{B}$ is calculated with the grid import flows $\mathbf{G}_{b,t}$, and the import cost $k_{b,t}^{\text{import}}$. The operating cost of production component $p \in \mathcal{P}$ is based on the production flow $\mathbf{P}_{p,b_{\text{ref}}(p),t}$ of the component's reference product $b_{\text{ref}}(p)$, and the component operating cost $k_p^{\text{operation}}$. Both $k_{b,t}^{\text{import}}$ and $k_p^{\text{operation}}$ include penalties for greenhouse gas emissions. Δ_t denotes the time step duration.

The base model decides on the energy system operation while satisfying the product balance constraints:

$$\mathbf{G}_{b,t} + \sum_{p \in \mathcal{P}} \mathbf{P}_{p,b,t} + \mathbf{S}_{s(b),t}^{\text{dis}} - \mathbf{S}_{s(b),t}^{\text{ch}} = d_{b,t} \quad \forall b \in \mathcal{B}, t \in \mathcal{T}. \quad (2)$$

$\mathbf{P}_{p,b,t}$ denotes the production flows to and from production components. $\mathbf{S}_{s(b),t}^{\text{dis}}$ and $\mathbf{S}_{s(b),t}^{\text{ch}}$ represent the storage inflows and outflows, respectively, and $d_{b,t}$ are the product demands. Each product is associated with a storage, denoted as $s(b)$.

We constrain the production limits of production components as well as their conversion efficiencies. Eq. (3) limits the reference product flow $\mathbf{P}_{p,b_{\text{ref}}(p),t}$ to the installed process capacity P_p^{nom} times the weather-dependent capacity factor $CF_{p,t}$. Eq. (4) models the part-load efficiency of production components with piecewise linear functions. For each segment $i \in \mathcal{J}$ of a piecewise function, Eq. (5) models the relation between the segment's product flows $\mathbf{P}_{p,b,i,t}^{\text{seg}}$ and the segment's reference product flow $\mathbf{P}_{p,b_{\text{ref}}(p),i,t}^{\text{seg}}$ with the coefficients $a_{p,i,b}$ and $c_{p,i,b}$. The binary $\delta_{p,i,t}$ indicates, whether segment i is active. Eqs. (6) and (7) ensure that a segment i is only active if $\mathbf{P}_{p,b_{\text{ref}}(p),t}^{\text{seg}}$ is between the segment's lower limit $L_{p,i}$ and upper limit $U_{p,i}$. At most one segment can be simultaneously active (Eq. (8)).

$$\mathbf{P}_{p,b_{\text{ref}}(p),t} \leq P_p^{\text{nom}} CF_{p,t} \quad \forall p \in \mathcal{P}, t \in \mathcal{T} \quad (3)$$

$$\begin{aligned}
 P_{p,b,t} &= \sum_{i \in \mathcal{J}} P_{p,b,i,t}^{\text{seg}} \quad \forall p \in \mathcal{P}, b \in \mathcal{B}, t \in \mathcal{T} & (4) \\
 P_{p,b,i,t}^{\text{seg}} &= a_{p,i,b} P_{p,b_{\text{ref}}(p),i,t}^{\text{seg}} + c_{p,i,b} \delta_{p,i,t} \quad \forall p \in \mathcal{P}, b \in \mathcal{B}, i \in \mathcal{J}, t \in \mathcal{T} & (5) \\
 \delta_{p,i,t} \cdot L_{p,i} &\leq P_{p,b_{\text{ref}}(p),i,t}^{\text{seg}} \quad \forall p \in \mathcal{P}, i \in \mathcal{J}, t \in \mathcal{T} & (6) \\
 P_{p,b_{\text{ref}}(p),i,t}^{\text{seg}} &\leq \delta_{p,i,t} U_{p,i} \quad \forall p \in \mathcal{P}, i \in \mathcal{J}, t \in \mathcal{T} & (7) \\
 \sum_{i \in \mathcal{J}} \delta_{p,i,t} &\leq 1 \quad \forall p \in \mathcal{P}, t \in \mathcal{T}. & (8)
 \end{aligned}$$

Furthermore, we constrain the storage operation. Eq. (9) couples the storage levels of consecutive time steps $SL_{s,t}$ and $SL_{s,t+1}$, while modeling charging efficiencies η_s^{ch} , discharging efficiencies η_s^{dis} , relative self-discharge efficiencies η_s^{self} , and static self-discharges S_s^{static} . Eqs. (10) and (11) limit the minimum and maximum storage levels, where SL_s^{nom} is the installed storage capacity. Eqs. (12) and (13) limit the maximum charging ($S_s^{\text{ch,max}}$) and discharging flows ($S_s^{\text{dis,max}}$). The binary charging ($\gamma_{s,t}^{\text{ch}}$) and discharging ($\gamma_{s,t}^{\text{dis}}$) decisions in Eq. (14) prohibit simultaneous charging and discharging.

$$\begin{aligned}
 SL_{s,t+1} &= SL_{s,t} (1 - \eta_s^{\text{self}}) - \Delta_t \cdot (S_{s,t}^{\text{ch}} \eta_s^{\text{ch}} - S_{s,t}^{\text{dis}} / \eta_s^{\text{dis}} - S_s^{\text{static}}) \quad \forall s \in \mathcal{S}, t \in \mathcal{T} & (9) \\
 0 &\leq SL_{s,t} \quad \forall s \in \mathcal{S}, t \in \mathcal{T} & (10) \\
 SL_{s,t} &\leq SL_s^{\text{nom}} \quad \forall s \in \mathcal{S}, t \in \mathcal{T} & (11) \\
 S_{s,t}^{\text{ch}} &\leq S_s^{\text{ch,max}} \cdot \gamma_{s,t}^{\text{ch}} \quad \forall s \in \mathcal{S}, t \in \mathcal{T} & (12) \\
 S_{s,t}^{\text{dis}} &\leq S_s^{\text{dis,max}} \cdot \gamma_{s,t}^{\text{dis}} \quad \forall s \in \mathcal{S}, t \in \mathcal{T} & (13) \\
 \gamma_{s,t}^{\text{ch}} + \gamma_{s,t}^{\text{dis}} &\leq 1 \quad \forall s \in \mathcal{S}, t \in \mathcal{T}. & (14)
 \end{aligned}$$

2.2 State-of-the-art-method to increase reliability with storage reserves

The base model presented in (Section 2.1) typically leads to operating schedules that frequently cycle storages to minimize operating cost. However, if storage levels are low, grid and component failures threaten the reliability of energy supply. To increase reliability, DMES operators can constrain storage reserves SL_s^{res} , which need to be maintained during failure-free operation:

$$\begin{aligned}
 \min \text{OPEX} &+ \sum_{t \in \mathcal{T}} \sum_{s \in \mathcal{S}} SL_{s,t}^{\text{slack}} \cdot k^{\text{pen}} & (15) \\
 \text{s.t.:} & \text{Eqs. (2) to (14), (16)} \\
 SL_s^{\text{res}} - SL_{s,t}^{\text{slack}} &\leq SL_{s,t} \quad \forall s \in \mathcal{S}, t \in \mathcal{T}. & (16)
 \end{aligned}$$

In case of failures, the storage reserves serve as backup storage (Mitra 2010). In general, higher storage reserves improve reliability. However, maintaining high storage reserves during failure-free operation is not always feasible, because serving peak demands requires discharging storages. To maintain feasibility of the optimization problem stated in Eq. (15), we introduce a slack variable $SL_{s,t}^{\text{slack}}$ in Eq. (16), which allows undercutting the storage reserves at a large penalty cost k^{pen} .

3 PARETO-OPTIMAL OPERATION CONSIDERING RELIABILITY AND COST

In this section, we propose a method to generate Pareto-optimal operating schedules regarding reliability and cost under grid and components failures. The method extends the base model for cost-optimization (Section 2.1) by three steps (Figure 1). Instead of constraining storage reserves (Section 2.2), we improve reliability by integrating an EENS approximation (Section 3.1) into the objective function of the base model. We solve the resulting bi-objective optimization model with a self-adjusting weighted sum algorithm (Section 3.2) that yields a set of Pareto-optimal operating schedules. However, the EENS approximation may be inaccurate. Therefore, Section 3.3 introduces a Monte Carlo reliability assessment (MCA), to provide DMES operators with an accurate EENS.

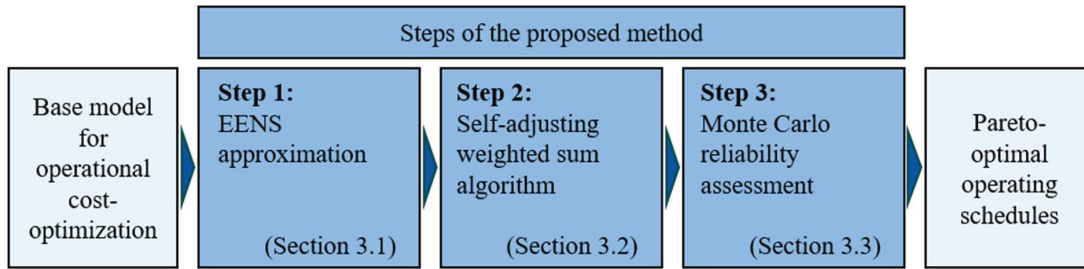


Figure 1: Overview of the proposed method to generate Pareto-optimal operating schedules regarding reliability and cost under grid and components failures.

3.1 EENS approximation

The EENS is a widely used energy system reliability metric describing the expected annual undersupply of energy demands. However, quantifying the EENS within an operational optimization model is challenging, because failures of grid utilities and components can occur at any time, and simultaneous failures are possible. Due to the combinatorial complexity and rarity of simultaneous failures, our EENS approximation focuses on non-simultaneous failures, i.e., N-1 failures (Hollermann et al. 2019). We approximate the EENS as:

$$EENS^{apr} = \sum_{t_F \in \mathcal{T}} \sum_{n \in \mathcal{N}} \sum_{b \in \mathcal{B}} (U_{t_F, n, b} \cdot \rho_n) \quad (17)$$

\mathcal{N} denotes the set of failure types, consisting of all grid utilities and production components with a non-zero failure probability ρ_n . During a failure of type n , the respective grid or production component is unavailable. $U_{t_F, n, b}$ quantifies the total undersupply of product b caused by a failure of type n at failure time t_F . $U_{t_F, n, b}$ considers undersupply on all time steps $\{t \mid t_F \leq t < t_R, t \in \mathcal{T}\}$ between the failure time t_F and the repair time $t_R = t_F + \Delta t_n$, where Δt_n is a predefined deterministic repair duration. However, our approach can be extended to consider multiple repair durations with individual probabilities for a given failure type.

Typically, the total undersupply $U_{t_F, n, b}$ decreases with increasing storage levels at failure time $SL_{s(b), t_F}$. We approximate this dependency with a univariate function F :

$$U_{t_F, n, b} = F(SL_{s(b), t_F}) \quad \forall t_F \in \mathcal{T}, n \in \mathcal{N}, b \in \mathcal{B}. \quad (18)$$

While the univariate function F results in low model complexity, it neglects that in sector-coupled energy systems, other storages apart from storage $s(b)$ can reduce the total undersupply of a product b . For example, during an electricity grid failure, stored electricity may not only reduce the total electricity undersupply but also the total cooling undersupply by powering compression chillers.

We motivate the definition of the function $F(SL_{s(b), t_F})$ with an exemplary energy system (Figure 2a) consisting of a cooling demand, two compression chillers, and a cold water storage. If one compression chiller fails, the potential supply $\tilde{p}_{b, t}$ of the remaining compression chiller is unable to meet the demand d_b (Figure 2b). Thus, undersupply $\tilde{u}_{b, t}$ occurs. The total undersupply $U_{t_F, n, b}$ tends to decrease with an increasing storage level at failure time $SL_{s(b), t_F}$. However, due to storage capacity limits, a minimum total undersupply $U_{t_F, n, b}^{\min}$ is unavoidable (Figure 2c). We define the storage level required to reach this minimum total undersupply as $SL_{t_F, n, b}^{\text{req}}$. If $SL_{s(b), t_F}$ is lower than $SL_{t_F, n, b}^{\text{req}}$, the total undersupply $U_{t_F, n, b}$ increases at most by a factor of the discharging efficiency η_s^{dis} (Figure 2d). We constrain this dependency with Eqs. (19) and (20):

$$U_{t_F, n, b} \geq U_{t_F, n, b}^{\min} + \eta_s^{\text{dis}} \left(SL_{t_F, n, b}^{\text{req}} - SL_{s(b), t_F} \right) \quad \forall t_F \in \mathcal{T}, n \in \mathcal{N}, b \in \mathcal{B} \quad (19)$$

$$U_{t_F,n,b} \geq U_{t_F,n,b}^{\min} \quad \forall t_F \in \mathcal{T}, n \in \mathcal{N}, b \in \mathcal{B}. \quad (20)$$

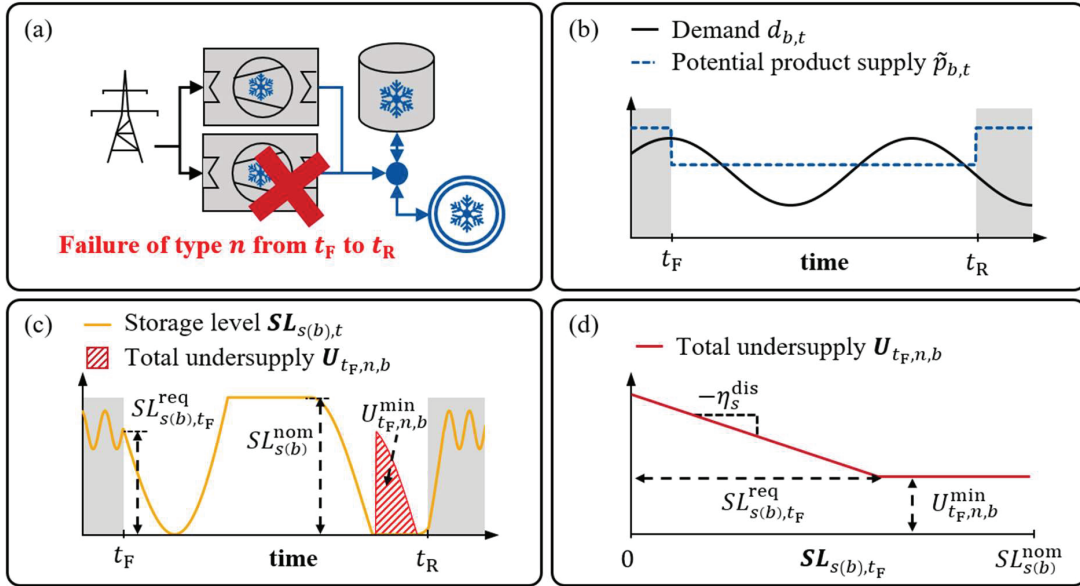


Figure 2: Exemplary illustration of the dependency of the total undersupply $U_{t_F,n,b}$ on the storage level at failure time $SL_{s(b),t_F}$. A compression chiller fails at t_F (a). During the failure, the potential supply $\tilde{p}_{b,t}$ of the remaining compression chiller is insufficient to meet the demand $d_{b,t}$ (b). Thus, the failure causes undersupply (c). While the total undersupply $U_{t_F,n,b}$ decreases with the storage level at failure time $SL_{s(b),t_F}$, a minimum total undersupply $U_{t_F,n,b}^{\min}$ is unavoidable due to storage capacity limits (d). $SL_{t_F,n,b}^{\text{req}}$ denotes the storage level that is required for the minimum total undersupply.

Approximating the $EENS^{\text{apr}}$ requires determining the parameters $U_{t_F,n,b}^{\min}$ and $SL_{t_F,n,b}^{\text{req}}$ for all failure times $t_F \in \mathcal{T}$, failure types $n \in \mathcal{N}$, and products $b \in \mathcal{B}$. To determine these parameters, we propose a heuristic approach, following the example in Figure 2. For a given failure time t_F , failure type n , and product p , we first determine the potential product supply $\tilde{p}_{b,t} \forall t \in \mathcal{T}_R := \{t \mid t_F \leq t < t_R, t \in \mathcal{T}\}$ that could be provided by the available production components (Figure 2b). Then, we employ a backward iteration algorithm, which requires a predefined storage level at repair time $\tilde{SL}_{s(b),t_R}$. The backward iteration algorithm computes the storage levels $\tilde{SL}_{s(b),t} \forall t \in \mathcal{T}_R$ and undersupply $\tilde{u}_{b,t} \forall t \in \mathcal{T}_R$ to determine $U_{t_F,n,b}^{\min}$ and $SL_{t_F,n,b}^{\text{req}}$ (Figure 2c).

In the following, we elaborate the details of our heuristic approach for energy systems with a single energy demand b . We first determine a suitable storage level at repair time $\tilde{SL}_{s(b),t_R}$, which is required to start the backward iteration (Section 3.1.1). Then, we discuss the potential product supply $\tilde{p}_{b,t}$ (Section 3.1.2) and the backward iteration algorithm (Section 3.1.3). Finally, we extend the heuristic approach to energy systems with multiple demands (Section 3.1.4).

3.1.1 Storage levels at repair time: The backward iteration requires a predefined storage level at repair time $\tilde{SL}_{s(b),t_R}$. While the backward iteration algorithm only considers undersupply during the failure, a low storage level $\tilde{SL}_{s(b),t_R}$ can cause undersupply after the repair due to upcoming peak-demands. To avoid undersupply after the repair, we set $\tilde{SL}_{s(b),t_R}$ to the storage level SL_{s,t_R} determined by solving the optimization problem stated in Eq. (21):

$$\min \sum_{s \in \mathcal{S}} \sum_{t \in \mathcal{T}} SL_{s,t} \quad (21)$$

s.t.: Eqs. (2) to (14).

Because Eq. (21) models the failure-free operation and prohibits undersupply, the resulting storage levels $SL_{s,t}$ are guaranteed to avoid undersupply after a repair.

3.1.2 Potential product supply: We determine the potential product supply $\tilde{p}_{b,t}$ for each failure time $t_F \in \mathcal{T}$, failure type $n \in \mathcal{N}$, and time step during the failure $t \in \mathcal{T}_R$. For energy systems with a single demand, $\tilde{p}_{b,t}$ is the maximum supply of product b that can be provided by all available production processes. Storages do not contribute to the potential product supply $\tilde{p}_{b,t}$. Notably, $\tilde{p}_{b,t}$ considers shortages of educts that are required to operate production components. For example, if the electricity grid fails in the exemplary energy system shown in Figure 2a, the potential supply of both compression chillers is zero.

3.1.3 Backward iteration algorithm: For each failure time $t_F \in \mathcal{T}$ and failure type $n \in \mathcal{N}$, we conduct a backward iteration over all time steps $t \in \mathcal{T}_R$, starting with time step $t_R - 1$. For each time step $t \in \mathcal{T}_R$, given the storage level $\widetilde{SL}_{s(b),t+1}$, we determine the minimum storage level $\widetilde{SL}_{s(b),t}$ required to minimize the undersupply $\tilde{u}_{b,t}$ at the current time step. After iterating over all time steps $t \in \mathcal{T}_R$, we calculate $SL_{t_F,n,b}^{req}$ and $U_{t_F,n,b}^{min}$ with Eqs. (22) and (23):

$$SL_{t_F,n,b}^{req} = \widetilde{SL}_{s(b),t_F} \quad \forall b \in \mathcal{B} \tag{22}$$

$$U_{t_F,n,b}^{min} = \sum_{t \in \mathcal{T}} \tilde{u}_{b,t} \quad \forall b \in \mathcal{B}. \tag{23}$$

We calculate the minimum undersupply $\tilde{u}_{b,t}$ and storage level $\widetilde{SL}_{s(b),t}$ required for this minimum undersupply by comparing the potential product supply $\tilde{p}_{b,t}$ to the demand $d_{b,t}$. If the demand $d_{b,t}$ exceeds the potential product supply $\tilde{p}_{b,t}$, minimizing the undersupply requires discharging the storage. With a predefined $\widetilde{SL}_{s(b),t+1}$, we calculate $\widetilde{SL}_{s(b),t}$ as:

$$\widetilde{SL}_{s(b),t} = \min \left\{ SL_{s(b)}^{nom}, \frac{\widetilde{SL}_{s(b),t+1} + \Delta_t \cdot S_{s(b)}^{static} + \Delta_t \cdot (d_{b,t} - \tilde{p}_{b,t}) / \eta_{s(b)}^{dis}}{(1 - \eta^{self})} \right\}. \tag{24}$$

Undersupply $\tilde{u}_{b,t}$ at the current time step t may be unavoidable because the storage level $\widetilde{SL}_{s(b),t}$ is limited to SL_s^{nom} . If the potential product supply $\tilde{p}_{b,t}$ exceeds the demand $d_{b,t}$, the undersupply $\tilde{u}_{b,t}$ is zero and the storage can be charged:

$$\widetilde{SL}_{s(b),t} = \max \left\{ 0, \frac{\widetilde{SL}_{s(b),t+1} + \Delta_t \cdot S_{s(b)}^{static} - \Delta_t \cdot (\tilde{p}_{b,t} - d_{b,t}) \cdot \eta_{s(b)}^{ch}}{(1 - \eta^{self})} \right\}. \tag{25}$$

For simplicity, Eqs. (24) and (25) neglect storage charging and discharging limits. If the storage charging limits are low, this negligence can result in an underestimation of the undersupply.

3.1.4 Extensions for energy systems with multiple demands: In energy systems with multiple demands, our heuristic faces an allocation problem for the potential product supply $\tilde{p}_{b,t}$ of a product b : $\tilde{p}_{b,t}$ can either serve the demand of product b , or can serve the demands of other products by supplying production components. For example, during a failure of the electricity grid, locally generated electricity can either supply electricity demands or provide cooling via compression chillers.

The allocation problem is solved by a demand hierarchy that needs to be predefined by DMES operators. For the product b_I with the highest priority in the demand hierarchy, we calculate SL_{t_F,n,b_I}^{req} and U_{t_F,n,b_I}^{min} as previously described. We then proceed with the next product b_{II} in the demand hierarchy. However,

the potential supply of production components that convert b_I to b_{II} may diminish, because b_I is partially used to serve the demand $d_{b_I,t}$. Thus, the potential product supply $\tilde{p}_{b_{II},t}$ reduces. For example, during a failure of the electricity grid, the potential cooling supply of compression chillers may reduce, if electricity demands are prioritized over cooling demands.

In summary, the presented heuristic approach determines the parameters $U_{t_F,n,b}^{\min}$ and $SL_{t_F,n,b}^{\text{req}}$ required to approximate the EENS within an operational optimization model.

3.2 Self-adjusting weighted sum algorithm

We integrate the EENS approximation into the objective function of the base model (Section 2.1). Then, we solve the resulting bi-objective optimization problem with a weighted sum method to generate multiple Pareto-optimal solutions. We choose the weighted sum method because it is compatible with the rolling horizon approach, which solves operational optimization problems with reduced computational time (Marquant et al. 2015). In this work, the weighted sum method solves the problem:

$$\begin{aligned} \min \omega_i \cdot \mathbf{OPEX} + (1 - \omega_i) \cdot \mathbf{EENS}^{\text{apr}} \\ \text{s.t.: Eqs. (2) to (14), (17), (19), (20).} \end{aligned} \tag{26}$$

The objective weight ω_i is updated in each iteration i , typically based on a user-defined set of weights. With a poorly defined set of objective weights, however, the weighted sum method is known to generate solutions, which are unevenly spaced in terms of the Euclidean distance between the normalized objective values of neighboring solutions (Marler und Arora 2010).

To generate evenly distributed solutions to the bi-objective problem (Eq. 26), we propose the self-adjusting weighted sum algorithm. In the first two iterations, it conducts single objective optimizations, setting the objective weight to $\omega_1 = 0$ and $\omega_2 = 1$, respectively. At the start of subsequent iterations, we identify the neighboring solutions m and n with the largest Euclidean distance between their normalized objective values. With the objective values \mathbf{OPEX} and $\mathbf{EENS}^{\text{apr}}$ of these neighboring solutions, we update the objective weight for the next iteration:

$$\omega_{i+1} = \left(1 - \frac{\mathbf{OPEX}_m - \mathbf{OPEX}_n}{\mathbf{EENS}_m^{\text{apr}} - \mathbf{EENS}_n^{\text{apr}}} \right)^{-1}. \tag{27}$$

The self-adjusting weighted sum algorithm repeatedly updates the objective weight ω_i and solves the optimization problem in Eq. (26) until reaching the desired number of Pareto-optimal solutions.

3.3 Monte Carlo reliability assessment

After determining Pareto-optimal operating schedules, we conduct Monte Carlo reliability assessments (MCAs) to evaluate the reliability of the operating schedules. In contrast to the EENS approximation presented in Section 2.2, the MCA considers simultaneous failures of multiple grid utilities or components. Furthermore, it employs optimization instead of heuristics to operate the DMES during failures. Thus, compared to the EENS approximation, the MCA evaluates the EENS of operating schedules with higher accuracy. While existing MCAs (Ren et al. 2022) assume that storages can be operated with perfect foresight of future failures, our proposed MCA avoids this prior knowledge to match real-world operation.

The proposed MCA generates a predefined number of failure scenarios $k \in \mathcal{K}$ with random failures according to the failure probabilities ρ_n and repair durations Δt_n . A failure scenario k has a yearly time horizon, in which multiple and simultaneous failures can occur. After scenario generation, the MCA iterates through all failure scenarios $k \in \mathcal{K}$ to calculate the $\mathbf{EENS}^{\text{MCA}}$ as the average undersupply over all scenarios.

To determine the undersupply during a failure scenario k , we iterate over each failure within the scenario in chronological order. We optimize each failure reaction to minimize the undersupply $\mathbf{u}_{b,t}$:

$$\min \sum_{t \in \mathcal{J}_T} \sum_{b \in \mathcal{B}} \mathbf{u}_{b,t} \quad (28)$$

s.t.: Eqs. (3) to (14), (29)

$$\mathbf{G}_{b,t} + \sum_{p \in \mathcal{P}} \mathbf{P}_{p,b,t} + \mathbf{S}_{s(b),t}^{\text{dis}} - \mathbf{S}_{s(b),t}^{\text{ch}} \geq d_{b,t} - \mathbf{u}_{b,t} \quad \forall b \in \mathcal{B}, t \in \mathcal{J}_T \quad (29)$$

To reduce the computational time required to optimize a failure reaction, we consider the reduced optimization horizon $\mathcal{J}_T := \{t \mid t_F \leq t < t_T, t \in \mathcal{J}\}$ with fixed storage levels at the failure time t_F and transition time t_T (Figure 3). The fixed storage level at t_F ensures non-anticipativity on the failure. The transition time step t_T denotes a time step after the repair time t_R , at which the failure reaction needs to match the planned operating schedule. A short transition period between the repair time t_R and the transition time t_T can lead to unnecessary undersupply. Thus, we set the transition period to the longest time required to charge all storages from their minimal to maximal storage level.

After optimizing a failure reaction, we update the planned operating schedule of the current failure scenario with the failure reaction. Since we chronologically iterate through all failures within a failure scenario k , the proposed MCA can consider subsequent and simultaneous failures.

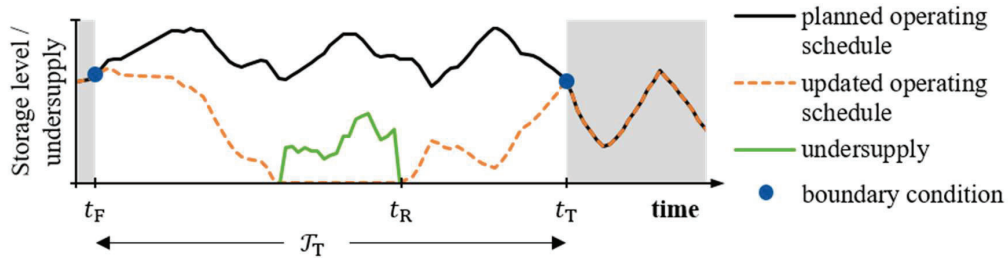


Figure 3: Exemplary illustration of a failure reaction optimized within the MCA to quantify the undersupply caused by a failure. Instead of the original time horizon \mathcal{J} , the MCA considers a reduced horizon \mathcal{J}_T to reduce computational times. During \mathcal{J}_T , the failure reaction is optimized to minimize undersupply. When optimizing the failure reaction, the storage levels at t_F and t_T are bound to the planned operating schedule. After optimization, the MCA updates the planned operating schedule with the failure reaction to consider subsequent failures.

4 CASE STUDY AND DISCUSSION

We apply the proposed method for the Pareto-optimal energy system operation under grid and component failures to a case study of an industrial energy system. Section 4.1 describes the case study. In Section 4.2, we compare the operating schedules generated by the proposed method to those generated by the state-of-the-art method. Section 4.3 analyzes the accuracy of the EENS approximation used within the proposed method.

4.1 Description of the industrial energy system model

The case study represents a partially decarbonized industrial energy system in 2030 with electricity, heating, and cooling demands (Figure 4). Reinert et al. (2023) describe the energy system model in detail. Electricity and natural gas prices average to 160 €/MWh and 60 €/MWh, respectively (Baumgärtner et al. 2019). The cost of greenhouse gas emissions is 130 €/t_{CO2-eq}. (IEA 2023)

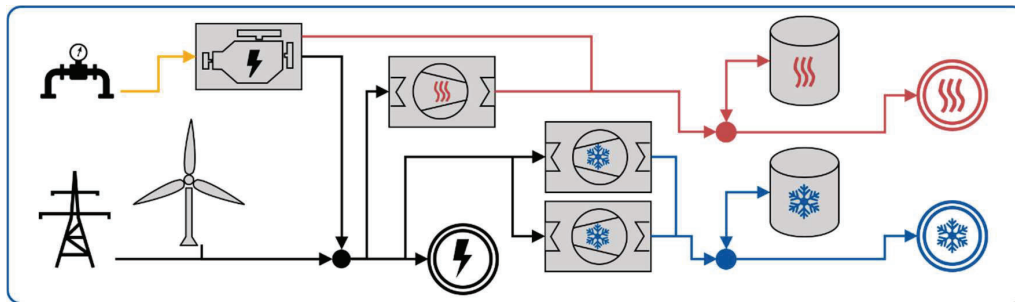


Figure 4: Overview of the considered industrial energy system.

Table 1 presents the installed capacities, failure probabilities, and repair durations of installed production components and the electricity grid. Due to limited data availability, we choose failure data for the heat pump and compression chillers that correspond to the failure data reported for absorption chillers (Jiang et al. 2018). The failure data of the electricity grid corresponds to many European countries (IEA 2023). We neglect failures of the natural gas grid due to their rarity (CEER 2023). Both heating and cooling storages have a capacity of 100 MWh each, with charging and discharging limited to 100 MW.

Table 1: Installed capacities, failure probabilities, and repair durations

Grid utility / Component	P_p^{nom} in MW	ρ_n in 1/h	Δt_n in h	Source
Electricity grid	-	$0.114 \cdot 10^{-3}$	2	CEER (2023)
Combined heat and power	3.04 (heating)	$0.335 \cdot 10^{-3}$	34	Jiang et al. (2018)
Heat pump	4.89	$0.219 \cdot 10^{-3}$	48	Own assumption
Compression chiller 1	4.46	$0.219 \cdot 10^{-3}$	48	Own assumption
Compression chiller 2	4.46	$0.219 \cdot 10^{-3}$	48	Own assumption
Wind turbine	19.46	-	-	-

4.2 Comparison of the Pareto-optimal to state-of-the-art operating schedules

In this section, we compare the Pareto-optimal operating schedules generated with the proposed method (M1-schedules, Section 3) with the operating schedules generated with the state-of-the-art method (M0-schedules, Section 2.2). We generate all schedules with a rolling horizon operational optimization, choosing an interval length of 168 h and a step size of 24 h, based on the parameter study of Marquant et al. (2015). We generate eleven M0-schedules, increasing the storage reserves $SL_s^{\text{res}} \forall s \in \mathcal{S}$ from 0 to 100 MWh in steps of 10 MWh while minimizing the OPEX. We generate ten M1-schedules with the self-adjusting weighed sum algorithm, simultaneously optimizing the EENS and OPEX. When approximating the EENS, we prioritize electricity supply over cooling supply over heating supply. To evaluate the reliability of all operating schedules, the MCA considers 2000 failure scenarios. 2000 failure scenarios lead to coefficients of variations below 0.05, which is a commonly used stopping criterion for Monte Carlo methods (Billinton und Li 1994; Da Silva et al. 2010). We solve all optimization models with Gurobi 10 (Gurobi Optimization 2023) to an optimality gap of 0.2 %.

The results show a significant trade-off between reliability and costs (Figure 5). Both the M0- and M1-schedules reach the minimum OPEX of 2725 k€/a. The M1-schedules achieve this minimum OPEX with an EENS of 36.3 MWh/a, improving the M0-schedule by 14.7 MWh/a. Starting from high EENS levels, reducing the EENS has a small impact on the OPEX. However, at lower EENS levels, further reducing the EENS considerably increases the OPEX. The minimum EENS is achieved when using M0 and setting the storage reserves to the storage capacities. This reduces the EENS by 58.2 % compared to the M1-schedule with minimum OPEX while increasing the OPEX by 24.8 %.

The M1-schedules fall short of the minimum EENS by 2.02 MWh/a because the underlying EENS approximation neglects simultaneous failures: The EENS approximation does not value charging storages above the storage levels required to cover N-1 failures. However, charging storages above this storage level further reduces undersupply in case of simultaneous failures. Because reducing the EENS progressively increases operating costs, falling short of the minimum EENS is only relevant, if undersupply causes high interruption cost. With the maximum interruption cost of 16.8 k€/MWh reported for industrial consumers (Wang et al. 2009), DMES operators would choose the marked operating schedules (Figure 6). Both the chosen M0- and the M1-schedule exceed the minimum EENS to reduce operating costs. Compared to the selected M0-schedule, the selected M1-schedule reduces the OPEX by 1.5 % and the EENS by 19.2 %.

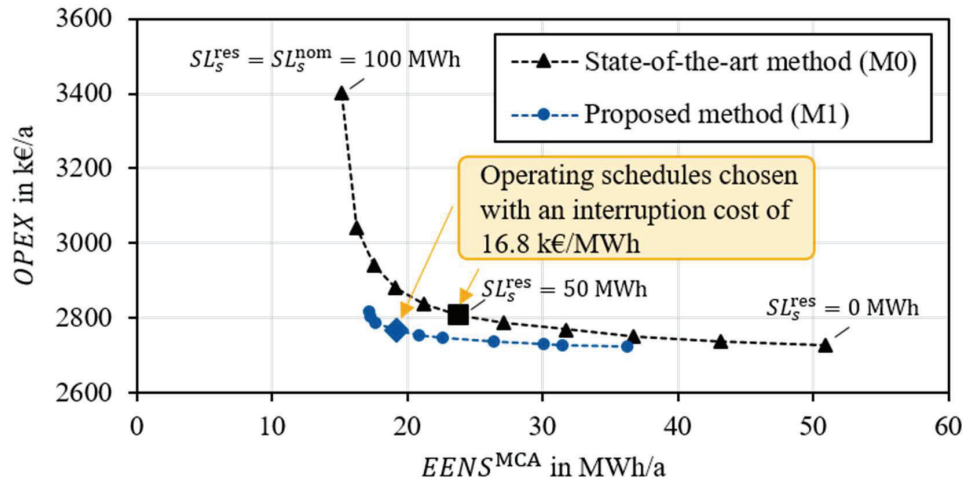


Figure 5: Comparison between the operating schedules generated with the state-of-the-art method (M0, Section 2.2) and the proposed method (M1, Section 3). The dotted lines provide visual guidance.

While the M0-schedules rely on increasing storage reserves SL_s^{res} to reduce the EENS, the M1-schedules were generated by simultaneously optimizing the EENS and OPEX within operational optimization. The M1-schedules generated in the first two iterations are not shown because they are dominated by solutions generated in subsequent iterations. With an interruption cost of 16.8 k€/MWh (Wang et al. 2009), DMES operators would choose the marked operating schedules.

4.3 Accuracy of the EENS approximation

To evaluate the accuracy of the EENS approximation by comparing it to the EENS evaluated with the MCA. We consider the M1-schedules discussed in Section 4.2. In the present case study, the EENS approximation consistently underestimates the EENS between 2.64 MWh/a to 3.73 MWh/a. Two opposing effects lead to this inaccuracy: While the EENS approximation overestimates the undersupply caused by N-1 failures, simultaneous failures of multiple grid utilities and components result in the overall underestimation. The error in the EENS approximation suggests that by refining this approximation, the trade-off between reliability and cost can be further improved. Furthermore, the error indicates that the MCA improves decision-making of DMES operators by providing more accurate reliability metrics.

5 CONCLUSION

The global transition towards volatile renewable energy supply requires significant energy storage capacities to synchronize energy demand and supply. However, integrating storages in distributed multi-energy systems (DMES) poses operational challenges, as operators need to carefully balance reliability and cost. Therefore, we propose a method for the Pareto-optimal operation of DMES including storages under grid and component failures. The method extends an operational cost-optimization model with an approximation of the Expected Energy Not Served, resulting in a bi-

objective problem. We solve the bi-objective problem with a self-adjusting weighted sum method before reevaluating the resulting operating schedules in a Monte Carlo reliability assessment.

In a case study of an industrial energy system, the proposed method reveals a significant trade-off between reliability and costs. The proposed method enables simultaneous cost and reliability improvements compared to maintaining predefined storage reserves. Thus, our work contributes to the economic and reliable storage operation. To further improve the trade-off between reliability and costs, future work should aim at refining the EENS approximation. The EENS approximation should value charging storages not only to prepare for N-1 failures but also for simultaneous failures. Furthermore, besides failures, DMES operators need to consider additional operation uncertainties, e.g., in energy demands or renewable availability. To consider these uncertainties, our method could be combined with stochastic operational optimization methods.

NOMENCLATURE

$a_{p,i,b}, c_{p,i,b}$	Linear function coefficients	–, MW
$CF_{p,t}$	Weather-dependent capacity factor	–
$d_{b,t}$	Demand	MW
EENS ^{apr}	Approximated Expected Energy Not Served	MWh/a
$G_{b,t}$	Gird import flows	MW
$k_p^{\text{operation}}, k_{b,t}^{\text{import}}$	Component operating cost, import cost of grid utilities	€/MWh
$L_{p,i}, U_{p,i}$	Lower and upper segment limits	MW
OPEX	Yearly operational expenditure	€/a
$P_{p,b,t}$	Production flows	MW
$P_{p,b,i,t}^{\text{seg}}$	Segment production flows	MW
p_p^{nom}	Nominal production capacity	MW
$S_{s,t}^{\text{ch}}, S_{s,t}^{\text{dis}}$	Storage inflows / outflows	MW
$S_s^{\text{ch,max}}, S_s^{\text{dis,max}}$	Charging / discharging limit	MW
$SL_{s,t}$	Storage level	MWh
$SL_{s,t}^{\text{slack}}$	Slack variable	MWh
$SL_{t_F,n,b}^{\text{req}}$	Required storage level for minimum total undersupply	MWh
S_s^{static}	Static storage losses	MW
$SL_{s,t}^{\text{nom}}, SL_s^{\text{res}}$	Storage capacity, storage reserve	MWh
$u_{b,t}$	Undersupply	MW
$U_{t_F,n,b}$	Total undersupply during repair time	MWh
$U_{t_F,n,b}^{\text{min}}$	Minimum total undersupply caused by a failure	MWh
$\gamma_{s,t}^{\text{ch}}, \gamma_{s,t}^{\text{dis}}$	Discharging / charging binary	–
$\delta_{p,i,t}$	Segment binary	–
Δ_n	Repair duration	h
Δ_t	Time step duration	h
$\eta_s^{\text{self}}, \eta_s^{\text{ch}}, \eta_s^{\text{dis}}$	Storage efficiencies	–
ρ_n	Failure probability	1/h
ω_i	Objective weight	–

Subscripts

$b \in \mathcal{B}$	Product	$p \in \mathcal{P}$	Production component
$i \in \mathcal{I}$	Piecewise linear segment	$s \in \mathcal{S}$	Storage
$k \in \mathcal{K}$	Failure scenario	$t \in \mathcal{T}$	Time slice
$n \in \mathcal{N}$	Failure type		

REFERENCES

- Baumgärtner, Nils; Delorme, Roman; Hennen, Maïke; Bardow, André (2019): Design of low-carbon utility systems: Exploiting time-dependent grid emissions for climate-friendly demand-side management. In: *Applied Energy* 247, S. 755–765. DOI: 10.1016/j.apenergy.2019.04.029.
- Billinton, Roy; Li, Wenyuan (1994): Reliability Assessment of Electric Power Systems Using Monte Carlo Methods. In: *Springer US*.
- CEER (2023): 7th CEER-ECRB Benchmarking Report on the Quality of Electricity and Gas Supply. Council of European Energy Regulators.
- Da Silva, A. M.L.; Fernandez, Reinaldo A. G.; Singh, Chanan (2010): Generating Capacity Reliability Evaluation Based on Monte Carlo Simulation and Cross-Entropy Methods. In: *IEEE Trans. Power Syst.* 25 (1), S. 129–137. DOI: 10.1109/TPWRS.2009.2036710.
- Guo, Yuanxiong; Zhao, Chaoyue (2018): Islanding-Aware Robust Energy Management for Microgrids. In: *IEEE Trans. Smart Grid* 9 (2), S. 1301–1309. DOI: 10.1109/TSG.2016.2585092.
- Gurobi Optimization, L. L.C. (2023): Gurobi 10: Gurobi Optimizer Reference Manual. <https://www.gurobi.com>.
- Hollermann, Dinah Elena; Hoffrogge, Dörthe Franzisca; Mayer, Fabian; Hennen, Maïke; Bardow, André (2019): Optimal (n-1)-reliable design of distributed energy supply systems. In: *Computers & Chemical Engineering* 121 (14), S. 317–326. DOI: 10.1016/j.compchemeng.2018.09.029.
- IEA (2023): Global Energy and Climate Model Documentation 2023. <https://www.iea.org/reports/global-energy-and-climate-model>.
- Jiang, Jinming; Wei, Xindong; Gao, Weijun; Kuroki, Soichiro; Liu, Zhonghui (2018): Reliability and Maintenance Prioritization Analysis of Combined Cooling, Heating and Power Systems. In: *Energies* 11 (6), S. 1519. DOI: 10.3390/en11061519.
- Marler, R. Timothy; Arora, Jasbir S. (2010): The weighted sum method for multi-objective optimization: new insights. In: *Struct Multidisc Optim* 41 (6), S. 853–862. DOI: 10.1007/s00158-009-0460-7.
- Marquant, Julien F.; Evins, Ralph; Carmeliet, Jan (2015): Reducing Computation Time with a Rolling Horizon Approach Applied to a MILP Formulation of Multiple Urban Energy Hub System. In: *Procedia Computer Science* 51, S. 2137–2146. DOI: 10.1016/j.procs.2015.05.486.
- Mitra, Joydeep (2010): Reliability-Based Sizing of Backup Storage. In: *IEEE Trans. Power Syst.* 25 (2), S. 1198–1199. DOI: 10.1109/tpwrs.2009.2037516.
- Pazouki, Samaneh; Haghifam, Mahmoud-Reza; Moser, Albert (2014): Uncertainty modeling in optimal operation of energy hub in presence of wind, storage and demand response. In: *International Journal of Electrical Power & Energy Systems* 61, S. 335–345. DOI: 10.1016/j.ijepes.2014.03.038.
- Reinert, Christiane; Nolzen, Niklas; Frohmann, Julia; Tillmanns, Dominik; Bardow, André (2023): Design of low-carbon multi-energy systems in the SecMOD framework by combining MILP optimization and life-cycle assessment. In: *Computers & Chemical Engineering*.
- Ren, Hongbo; Jiang, Zipei; Wu, Qiong; Li, Qifen; Yang, Yongwen (2022): Integrated optimization of a regional integrated energy system with thermal energy storage considering both resilience and reliability. In: *Energy* 261, S. 125333. DOI: 10.1016/j.energy.2022.125333.
- Wang, P.; Goel, L.; Ding, Y. (2009): Reliability assessment of restructured power systems using optimal load shedding technique. In: *IET Generation, Transmission & Distribution* 3 (7), S. 628–640. DOI: 10.1049/iet-gtd.2008.0308.

ACKNOWLEDGEMENTS

We gratefully acknowledge the financial support from the German Federal Ministry of Education and Research in the funding initiative “KMU-innovativ” via the project Be-Safe (01LY2117-D). Simulations were performed with computing resources granted by RWTH Aachen University under project thes1513.